Nucleic Acids Research, 2006, Vol. 34, No. 11 ***3201–3208***
doi:10.1093/nar/gkl413

Multiple-turnover thio-ATP hydrolase and phospho-enzyme intermediate formation activities catalyzed by an RNA enzyme

Dayal Saran[1,3,4], Daniel M. Held[2,3,4] and Donald H. Burke[3,4,*]

[1]Department of Chemistry and [2]Department of Biology, Indiana University, Bloomington, IN 47405, USA, [3]Department of Molecular Microbiology and Immunology and [4]Department of Biochemistry, University of Missouri School of Medicine, Columbia, MO 65211, USA

Received March 1, 2006; Revised April 25, 2006; Accepted May 19, 2006

ABSTRACT

Ribozymes that phosphorylate internal 2′-OH positions mimic the first mechanistic step of P-type ATPase enzymes by forming a phospho-enzyme intermediate. We previously described 2′-autophosphorylation and autothiophosphorylation by the 2PTmin3.2 ribozyme. In the present work we demonstrate that the thiophosphorylated form of this ribozyme can de-thiophosphorylate in the absence of ATPγS. Identical ionic conditions yield a thiophosphorylated strand when ATPγS is included, thus effecting a net ATPγS hydrolysis. The de-thiophosphorylation step is nearly independent of pH over the range of 6.3–8.5 and does not require a specifically folded RNA structure, but this step is greatly stimulated by transition metal ions. By monitoring thiophosphate release, we observe 29–46 ATPγS hydrolyzed per ribozyme strand in 24 h, corresponding to a turnover rate of 1.2–2.0 h^{-1}. The existence of an ATP- (or thio-ATP-)powered catalytic cycle raises the possibility of using ribozymes to transduce chemical energy into mechanical work for nucleic acid nanodevices.

INTRODUCTION

Ribozymes isolated through *in vitro* selection catalyze reactions ranging from ligation and peptide bond formation to oxidation/reduction and Michael addition (1–5). Efforts are under way in several laboratories to use *in vitro* selected ribozymes to understand intrinsic constraints for RNA World evolution and to create artificial metabolisms either in extant cells or in artificial cells. Fully artificial ribozymes and aptamers can also be harnessed for the fabrication of molecular scale mechanical devices and to improve chemical process engineering. For example, the Lu group has described lead-sensing DNAzymes (6) and aptamer-conjugated gold nanoparticles that act as biosensors for free ATP (7), and the Jaeschke group has described enantioselective synthesis of a Diels–Alder cycloaddition product by passing substrates over a catalytic column of immobilized Diels-Alderase ribozyme (8–11). Ribozymes that transduce stored chemical energy into multiple cycles of mechanical work would represent a significant advance in nucleic acid nanotechnology.

An important function of enzymes is to capture stored chemical energy to drive thermodynamically unfavorable processes, such as a disfavored chemical transformation or the production of mechanical work. A common energy source for cellular enzymes is the hydrolysis of the β–γ phosphoanhydride bond of nucleotide triphosphates to yield the nucleotide diphosphate and inorganic phosphate. Nitrogenase reductase and receptor-coupled GTPases and other enzymes exploit differential binding energy between the NTP and NDP to drive conformational changes that either activate or inactivate the enzyme. Similarly, covalent phosphorylation regulates many enzymes, or drives conformational changes that yield mechanical work. The reversibility of such phosphorylation is essential for biologically responsive enzyme regulation and for completing the work cycle for energy-transducing molecular motors. The P-type ATP hydrolase enzymes comprise a large protein family of ATPases that generate essential ion gradients, which are the basis for such diverse functions as signaling, energy storage and secondary transport. They form a phosphorylated enzyme intermediate during ion transport (hence the name 'P-type'), and then hydrolyze the phosphate to return to their resting conformation.

We previously described a set of ribozymes that were selected for autothiophosphorylation activity (12). The RNAs in the selected population use either ATP or ATPγS to (thio)phosphorylate internal 2′ hydroxyls, leading to the accumulation of (thio)phospho-ribozyme products. A truncated form of one of these ribozymes was separated into a 27 nt catalytic strand (2PTmin3.2) and a 26 nt substrate strand. Replacing most of the ribose with deoxyribose yielded

*To whom correspondence should be address. Tel: +1 573 884 1316; Fax: +1 573 884 9676; Email: burkedh@missouri.edu

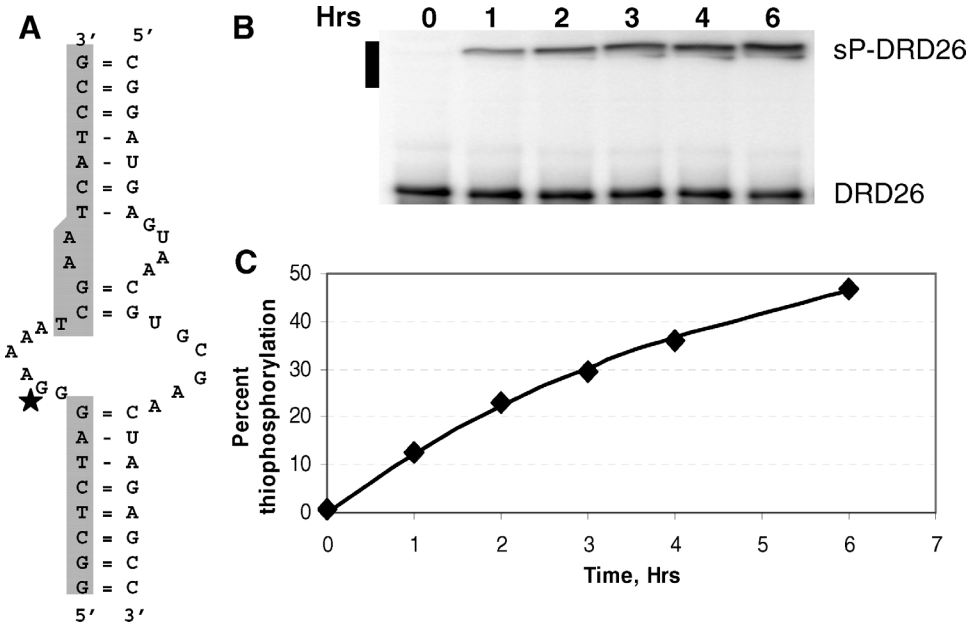

Figure 1. Phosphorylation. (**A**) Secondary structure of the ribozyme/substrate complex. Shaded positions are deoxynucleotides. The site of phosphorylation on the guanosine at position 10 of the substrate strand ($G10_S$) is indicated by the star. (**B**) Autoradiograph of product accumulation from the thiophosphorylation reaction. Incubation times (hrs) are indicated above each lane. Black bar on the left indicates the location and thickness of the organomercurial (APM) layer. (**C**) Plot of thiophosphorylated product accumulation versus time. Smooth curve is a best fit of the data to a single-exponential curve $F_t = F_\infty(1 - e^{-kt})$, where F_t and F_∞ are the percent RNA thiophosphorylated at time 't' and at infinite time, respectively, and k is the observed rate constant.

a chimeric DNA–RNA–DNA species (DRD26) wherein eight ribonucleotides are flanked by deoxynucleotides on both sides. Detailed analysis of this complex mapped the site of phosphorylation to the second (G) within the unpaired sequence 5′-G**G**AAAA-3′ of DRD26 (Figure 1). Most of the deoxynucleotides of the substrate strand can be replaced by other nucleotides as long as Watson–Crick base pairing is maintained (12). In the present work we demonstrate that the 2PTmin3.2/DRD26 complex can release its covalent modification through hydrolysis. We first delineate the parameters that control this hydrolysis, then establish that the complex can participate in multiple cycles of thiophosphorylation and de-thiophosphorylation, thereby acting as a thio-ATPase (thio-ATP hydrolase). Because the catalytic cycle includes a thiophospho-ribozyme intermediate, this complex can loosely be thought of as a P-type riboATPase.

MATERIALS AND METHODS

Materials

Oligonucleotides were purchased from Integrated DNA Technologies or were transcribed *in vitro* from synthetic templates. Ribozyme strand 2PTmin3.2 gave equivalent results when used as synthetic strand or when purified from *in vitro* transcriptions. ATPγS was purchased from Sigma, [γ-^{32}P]ATP was purchased from MP Biomedicals.

(thio)Phosphorylation and de-thiophosphorylation

Substrate strands were 5′ radiolabeled with ^{32}P by incubating the initial strand with [γ-^{32}P]ATP and T4 polynucleotide kinase. Ribozyme-catalyzed auto-(thio)phosphorylation reactions were performed under conditions described previously (12). In brief, the two strands of the complex were denatured at 82°C in a solution containing monovalent ions and pH buffer, allowed to cool, and then divalent metal ions were added. Final composition of the 'selection buffer' is 20 mM Mg^{2+}, 5 mM Ca^{2+}, 2.5 mM Mn^{2+}, 10 μM each for Co^{2+}, Cu^{2+}, Zn^{2+} and Ni^{2+}, 50 mM K^+, 150 mM Na^+ in 50 mM PIPES buffer at pH 6.4. Reactions were initiated by addition of ATPγS to a final concentration of 5 mM, stopped by addition of denaturing gel-loading buffer and quickly frozen at −80°C. De-thiophosphorylation reactions were performed by first purifying the thiophosphorylated substrate strand from the APM layer of a trilayer organomercurial gel (12,13) and then incubating the thiophosphorylated substrate strand DRD26 with or without the ribozyme strand 2PTmin3.2 under similar buffer conditions to those in which it had been thiophosphorylated except as noted in the text. All reactions were performed at 37°C unless otherwise noted. The fraction of the input material that had become de-thiophosphorylated at each time point was determined by separating the reaction products on a trilayer APM gel, exposing the dried gel to a phosphorimager screen (Typhoon, Molecular Dynamics), and quantifying the fraction in the APM layer using ImageQuant software.

Multiple-turnover ATPase activity analysis

To monitor ribozyme-catalyzed thiophosphate release, active complex was assembled by annealing 25 μM DRD26 and 75 μM 2PTmin3.2 in selection buffer with 5 mM ATPγS and incubated overnight. Control reactions included all-DNA versions of both strands. Samples were removed at 0, 3, 7, 11, 14 and 24 h, and quenched by rapid freezing on

dry ice. Assays for free thiophosphate used malachite green, which is a dye that has been shown previously to exhibit greatly increased absorbance at 650 nm upon binding to inorganic phosphate. Calibration with Na_3PO_3S showed a similar linearity for thiophosphate (inset in Figure 6). For each time point from the RNA-catalyzed reactions, 2 µl of the reaction mixture was diluted to 800 µl, followed by addition of 200 µl of malachite green solution supplied in the kit (Bioassay Systems). This dilution brought the free thiophosphate concentration into the linear range of the assay (0.1–5 µM) and prevented metal ion-induced precipitation of Malachite Green at concentrations of free phosphate above 10 µM. Dilution mixtures were incubated at room temperature for 11 min before measuring absorbance at 650 nm. Absorbance was converted to the concentration of the thiophosphate in the experimental sample using the linear relation between absorbance and concentration. To keep the final thiophosphate concentrations within the linear range of the assay, the 14 and 24 h time points were diluted 500 and 600 times and therefore a correction factor of 1.25 and 1.5 was applied to these time points in Figure 6. The commercial ATPγS (90% purity) contained a significant amount of ADP (by high-performance liquid chromatography, data not shown) and free thiophosphate, presumably from hydrolysis.

RESULTS

Phosphorylation and de-thiophosphorylation of substrate strand

When ribozyme 2PTmin3.2 is annealed with 5′ radiolabeled substrate strand DRD26 and incubated in 5 mM ATPγS, thiophosphorylation of the substrate proceeds with a first-order rate constant, $k_{obs} \approx 0.21\ h^{-1}$, similar to values obtained previously (12). Thiophosphorylated DRD26 was purified from the organomercurial layer of a trilayer gel containing acryloylamino-phenylmercuric chloride (APM) (13,14), annealed to ribozyme strand, and incubated in selection buffer in the presence of 5 mM ADP. When the products of this reaction were separated on a second trilayer organomercurial gel, the fraction of the radioactivity that shifted into the APM layer decreased with time, indicating loss of thiophosphate from the radiolabeled strand (Figure 2A, diamonds, and Figure 2B). Interestingly, there is a highly reproducible lag in the reaction, with little de-thiophosphorylation occurring within the first hour followed by an increased rate of loss of thiophosphate. Similar biphasic kinetics were observed throughout this study.

To discern whether the loss of thiophosphate from the DRD26 strand indicates thiophosphate hydrolysis or ATPγS synthesis, thiophosphorylated RNA was incubated in selection buffer either with or without ribozyme (no ADP in either reaction). De-thiophosphorylation kinetics under these conditions were essentially identical to those observed for the complete reaction (Figure 2A, circles and triangle). The substrate strand is predicted to be able to form alternative dimerized structures with as many as 10 Watson–Crick base pairs. Several of these structures place the thiophosphorylated nucleotide in a structural context that is similar to that of the ribozyme–substrate complex (Figure 2D). To rule out the possibility that alternative structures were responsible

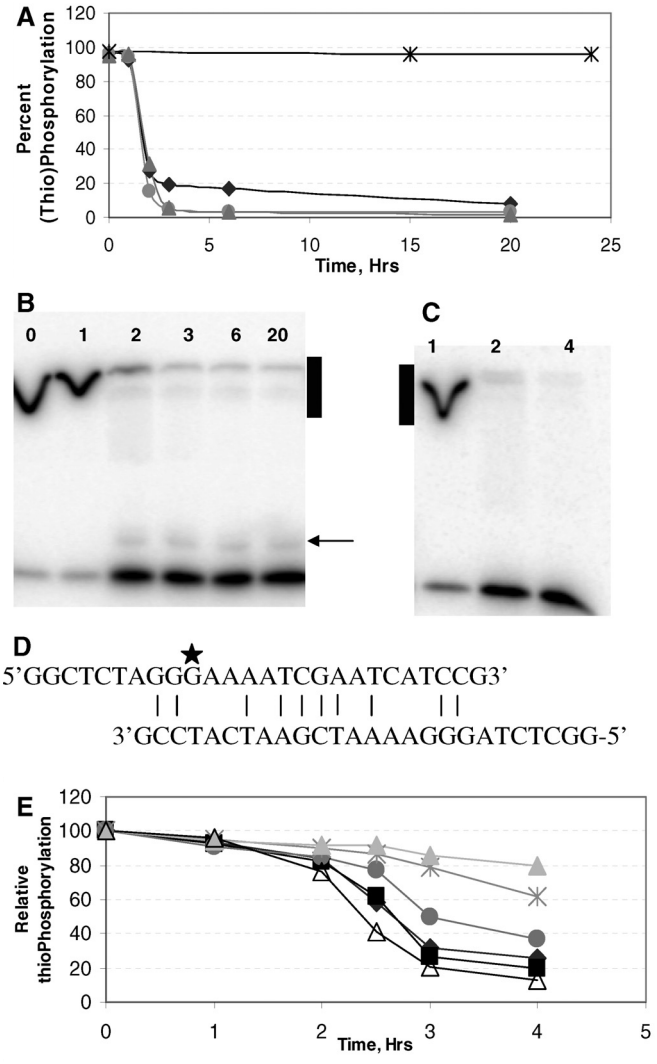

Figure 2. De-thiophosphorylation. (**A**) The percent of DRD26 in the (thio)phosphorylated form (i.e. unreacted) is plotted as a function of time for substrate strand incubated in the presence of ribozyme 2PTmin3.2 and ADP (diamonds), ribozyme only (circles), or by itself (triangles). Asterisk represents the de-thiophosphorylation of substrate strand DRD26 that had been auto-phosphorylated at $G10_S$ by [^{32}P]ATP. (**B**) and (**C**) Autoradiographs of typical gels showing loss of thiophosphoryl group from end-labeled RNA in the absence (B) or presence (C) of the reducing agent tris-carboxyethylphosphine (TCEP) (13). De-thiophosphorylation times in hrs are indicated above each lane. A weak oxidized dimer product just above the de-thiophosphorylated monomer is evident at long times when TCEP is omitted. Black bars indicate locations and thicknesses of APM layers. (**D**) Predicted structure of potential dimer of the substrate strand. (**E**) Concentration dependence. De-thiophosphorylation of 0.5 µM substrate strand was monitored in the presence of 0 (diamonds), 0.5 µM (squares), 1 µM (circles), 1.5 µM (asterisks) and 2 µM (solid triangles) unlabeled substrate strand DRD26. De-thiophosphorylation of 2.5 µM substrate strand was also monitored in the presence of 10 µM ribozyme strand (open triangles).

for the ribozyme-free reaction observed in Figure 2A, de-thiophosphorylation of 0.5 µM radiolabeled DRD26 strand was monitored in the presence of increasing concentrations of unlabeled DRD26. Rather than promoting the reaction, the unlabeled strand was inhibitory, with little de-thiophosphorylation observed when the total DRD26 concentration reached 2.5 µM (Figure 2E). In contrast,

de-thiophosphorylation proceeded normally when dimerization was prevented by including 10 μM ribozyme strand along with 2.5 μM DRD26 (Figure 2E, open triangles), or when DRD26 was annealed to a fully complementary DNA oligonucleotide (data not shown). Normal de-thiophosphorylation was also observed when the substrate strand was incubated alone in the presence of 8 M urea (data not shown). Taken together with the results of Figure 2A, these results indicate that de-thiophosphorylation is most efficient in unstructured RNA, that substrate self-dimerization is inhibitory, and that the reaction does not require either ADP or the folded secondary structure of the assembled complex, although it can be inhibited by some specific secondary structural contexts (potential self-dimers).

Temperature and pH dependence of the de-thiophosphorylation reaction

When DRD26 de-thiophosphorylation kinetics were monitored over the temperature range of 20–55°C, the amount of de-thiophosphorylation after 4 h increased with increasing temperature (Figure 3A). Some of this effect may be due to enhanced intrinsic chemical reactivity with increasing temperature. However, the magnitude of the de-thiophosphorylation increased markedly between 30 and 40°C (Figure 3B). This apparently cooperative transition supports a model in which inhibitory secondary structures melt over this range to expose the 2′-thiophosphate to hydrolysis. The shortening of the lag phase of the reaction at elevated temperatures is especially evident when yield after 2 h is compared across the temperature range (Figure 3B, circles).

When the pH of de-thiophosphorylation reactions was increased from 6.3 to 8.5, there was only a slight diminution (~20%) in the extent of the reaction after 4 h at the highest pH values, in spite of the >150-fold increase in hydroxide ion concentration over this pH range (Figure 3C). Thus, proton transfer does not control the rate of de-thiophosphorylation. If the chemical step of the reaction determines the rate, these observations are consistent with an S_{N1}-like, dissociative reaction mechanism in which the limiting step is the formation of a planar, metaphosphate transition state, rather than the deprotonation of an attacking nucleophile such as water. Consistent with this model, hydrolysis of organic phosphate monoesters—such as sugar phosphates, serine or tyrosine phosphates and the γ-phosphoryl group of ATP in aqueous solution—also progresses through a predominately dissociative reaction pathway that is largely independent of pH (15–18). Alternatively, the rate limiting step for de-thiophosphorylation of DRD26 may be a slow, pH-independent conformational change that occurs prior to the chemical step.

Metal ion dependence of the de-thiophosphorylation reaction

De-thiophosphorylation of the DRD26 strand was carried out in the presence of several combinations of metal ions. In the first series of reactions, the concentrations of all the divalent metal ions were gradually increased to triple that of the original selection buffer. Over this concentration range there is little change in de-thiophosphorylation, although the overall trend is toward slightly reduced rates and reduced

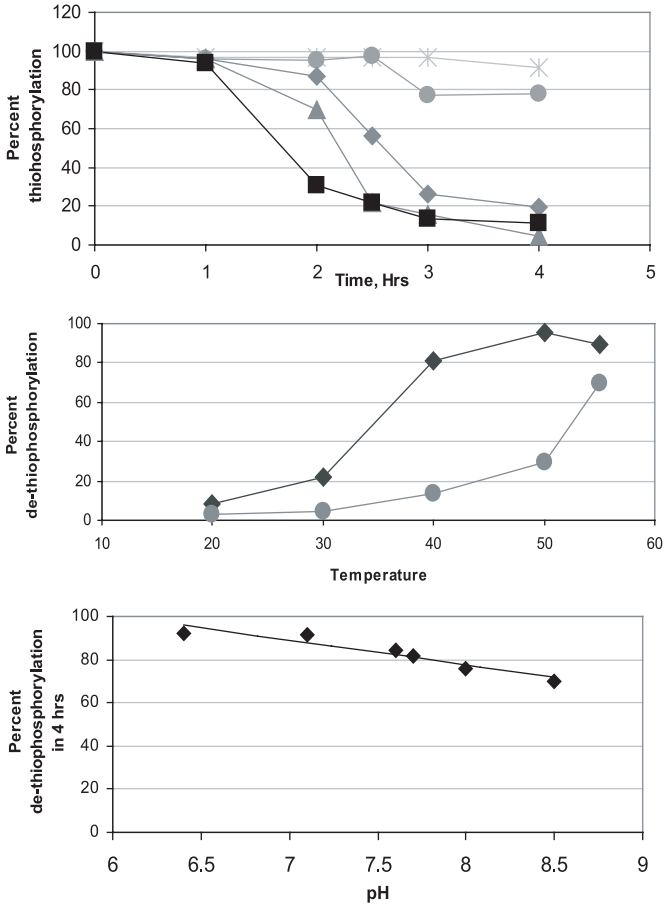

Figure 3. Temperature and pH dependence of de-thiophosphorylation reaction. (**A**) De-thiophosphorylation of substrate strand DRD26 was monitored at 20°C (asterisk), 30°C (circle), 40°C (diamond), 50°C (triangle) and 55°C (square). (**B**) Fraction de-thiophosphorylated at 2 h (circles) or 4 h (diamonds) is plotted as a function of the temperature of the reaction, or (**C**) as a function of pH. Reactions carried out at pH 6.4, 7.1 and 7.6 used 50 mM PIPES as the pH buffer; those carried out at pH 7.7, 8.1 and 8.5 used 50 mM Tris–HCl.

final extent of the reaction at the highest divalent ion concentration (Figure 4A). The second series of reactions included various subsets of the ions from the selection buffer, each at their original concentrations. When all components were present, de-thiophosphorylation was essentially complete by 5 h. Both the rate and the final extent of de-thiophosphorylation was reduced when all of the trace transition metals (Zn^{2+}, Co^{2+}, Ni^{2+}, Cu^{2+}) were omitted. Further reductions were observed when Mn^{2+} or all added divalent ions were omitted (Figure 4B). Interestingly, Mg^{2+} by itself appeared to protect against de-thiophosphorylation (Figure 4B, compare diamonds and crosses). For the third set of reactions, the trace transition metal ions were omitted individually while the others were maintained at a combined total of 40 μM. All the other components of the reaction mixture were unaltered. Reactions that included combinations of two or three of the trace transition metal ions yielded complete de-thiophosphorylation of the substrate strand within 4 h. Interestingly, the de-thiophosphorylation yield was reduced by nearly half when only one trace metal was included at a time (Figure 4C). Finally, in the fourth set of

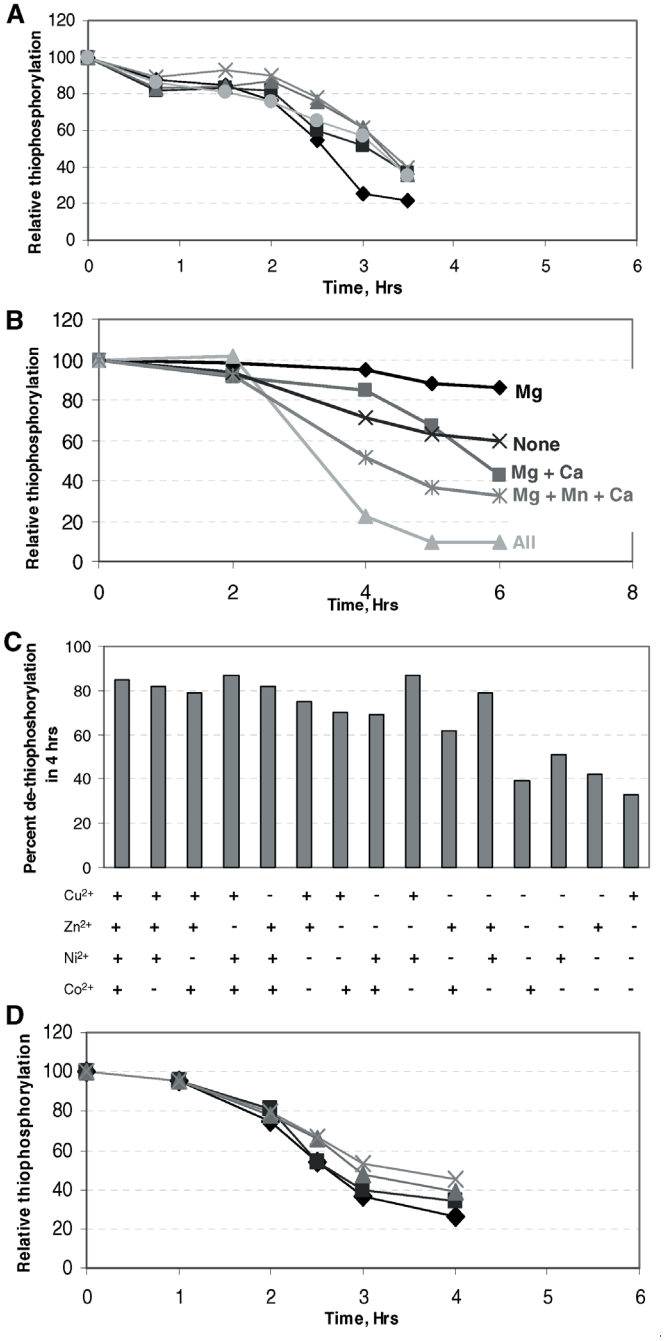

Figure 4. Metal ion dependence. De-thiophosphorylation was monitored under several ionic conditions. (**A**) Reactions were carried out in original selection buffer (diamonds), or in solutions at 1.25-fold (squares), 1.5-fold (triangles), 2-fold (crosses) or 3-fold (circles) increased concentrations. (**B**) Reactions were carried out in solutions containing the indicated divalent ions in addition to the other components of selection buffer. (**C**) Reactions were carried out in selection buffer in which trace transition metal ions were included in the combinations indicated, in each case at a total concentration of 40 μM. (**D**) Reactions were carried out in increasing concentrations of Ni^{2+}, Cu^{2+}, Co^{2+} and Zn^{2+}, each at 10 μM (diamonds), 15 μM (squares), 20 μM (triangles) or 25 μM (asterisks).

reactions, the total transition metal ion concentration was increased from 40 to 100 μM, again with the other reaction components unaltered (Figure 4D). For each reaction in this set, a similar sigmoidal pattern is observed, with slightly

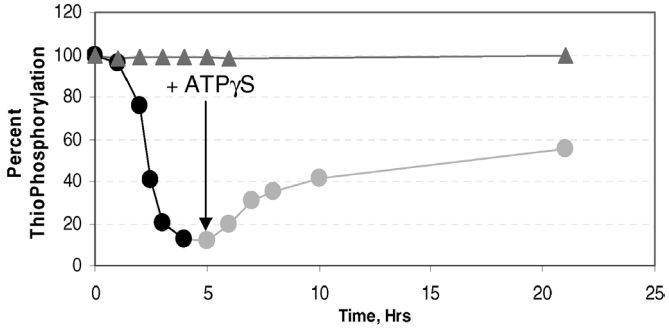

Figure 5. De-thiophosphorylation and re-thiophosphorylation. Percent DRD26 de-thiophosphorylated at various times is plotted for reactions initially without ATPγS (black circles) followed by addition of ATPγS to a final concentration of 5 mM after 5 h (grey circles), or in which 5 mM ATPγS is present throughout (triangles).

lesser extent of de-thiophosphorylation with increasing concentrations of transition metal ions, possibly due to non-specific binding of these soft metal ions to soft ligands in the RNA. Thus, the de-thiophosphorylation reaction depends heavily on the combination of metal ions present, with significant stimulation by low concentrations of the trace transition metals, slight reduction of yield at higher concentrations, some dependence on the identity of the transition metal ion utilized, and apparent protection by Mg^{2+}.

De-thiophosphorylation and re-thiophosphorylation

If the de-thiophosphorylation reaction is a simple hydrolysis, it should regenerate the original DRD26 strand, which should then be capable of re-thiophosphorylation with ATPγS. To test this hypothesis, ribozyme/substrate complex was allowed to de-thiophosphorylate for 5 h, after which ATPγS was added to a final concentration of 5 mM (Figure 5). Re-thiophosphorylation kinetics during the second phase of the reaction were nearly identical ($k = 0.24\ h^{-1}$; plateau value 55%) to those observed when naïve complex was incubated with ATPγS (compare with Figure 1C). Thus, the de-thiophosphorylation reaction does not damage or modify the DRD26 strand in any way that impedes its reactivity with ATPγS. Surprisingly, a parallel reaction that included ATPγS from the beginning showed no change in DRD26 thiophosphorylation over the course of the reaction (Figure 5, triangles). The fact that this mixture does not de-thiophosphorylate to the same 60% value obtained upon thiophosphorylation of naïve or fully de-thiophosphorylated species may suggest conformational dynamics of the annealed complex (see discussion).

A multiple-turnover thio-ATPase ribozyme (ribo thioATPase)

The data above suggest that the complex is capable of undergoing multiple cycles of de-thiophosphorylation and re-thiophosphorylation at the expense of ATPγS, thereby acting as a multiple-turnover thio-ATPase ribozyme (ATPγS hydrolase). To test this possibility directly, inorganic thiophosphate release was monitored using malachite green, a dye that exhibits greatly increased absorbance at 650 nm upon binding to inorganic phosphate (19–21). We find that the response of the malachite green signal is also linear with thiophosphate

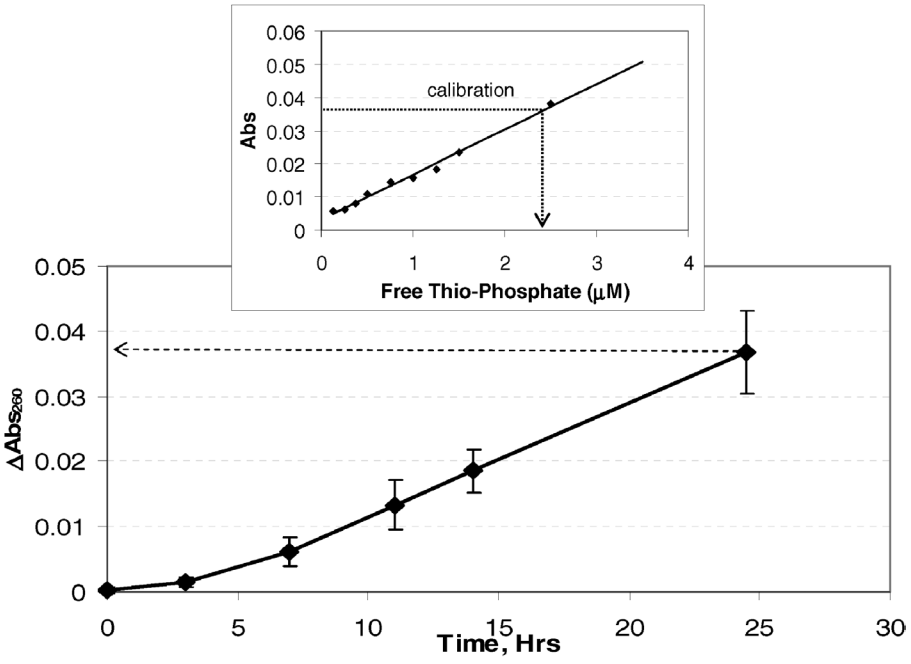

Figure 6. ATPase activity. Difference in the malachite green absorbance (ΔAbs_{650}) indicating released thiophosphate in the experimental sample versus the control is plotted with respect to time. Samples were collected at 0, 3, 7, 11, 14 and 24 h. Uncertainties reflect standard deviations among four replicate samples. Calibration curve (inset) shows the linear increase in the absorbance with increasing concentrations of free thiophosphate. For the 24 hr sample, ΔAbs_{650} reached 0.0365 ± 0.0064, representing a free thiophosphate concentration of 2.35 ± 0.057 μM. Correcting for the 400-fold sample dilution into the linear range of the assay yields 940 ± 230 μM excess free thiophosphate in the experimental sample versus the control.

concentration (inset in Figure 6), making it appropriate for monitoring thiophosphate release from ATPγS.

Unlabeled substrate strand DRD26 and ribozyme strand 2PTmin3.2 were annealed and incubated overnight in selection buffer with 5 mM ATPγS. A parallel reaction in which both strands were present in all-DNA (inactive) form was included as control. Aliquots were taken from both reactions at various times, diluted to the linear concentration range of the malachite green assay and monitored spectrophotometrically for free thiophosphate. The excess of released thiophosphate in the experimental sample versus the control increased with time (Figure 6). After a short lag, product formation was linear during the 24 h of the assay and showed no sign of plateauing. These observations are consistent with a model in which the annealed complex was actively liberating thiophosphate from ATPγS via a thiophospho-ribozyme intermediate. By the end of the assay, free thiophosphate concentrations reached 940 ± 230 μM. Because the ribozyme/substrate complex was only 25 μM, this indicates that the complex had catalyzed 29–46 turnovers in 24 h, corresponding to a net ATPγS hydrolysis rate of 1–2 h^{-1}. The annealed ribozyme/substrate complex is therefore a multiple-turnover thio-ATP hydrolase.

DISCUSSION

Multiple-turnover catalysis

In addition to the originally selected autothiophosphorylation activity of ribozyme 2PTmin3.2 (12), we show here that this ribozyme undergoes multiple cycles of thiophosphorylation/de-thiophosphorylation to yield a net conversion of ATPγS into ADP and thiophosphate (riboATPγS hydrolase). The reaction generates a thiophospho-ribozyme intermediate, leading us to refer to the annealed complex as a 'P-type riboATPase (thio-ATP hydrolase) ribozyme.' Formation of the thio-phosphoribozyme intermediate requires divalent metal ions (12) and is inhibited by ADP (data not shown), while thiophosphate hydrolysis yields the original complex.

The multiple turnover nature of this complex is fundamentally different from that of previously described *trans*-acting ribozymes. For example, the catalytic cycle of ribozyme Kin.46 is defined by five steps: (i) annealing of a 7 nt RNA substrate to an internal guide sequence in the ribozyme, (ii) binding of ATP (or ATPγS), (iii) (thio)phosphoryl transfer to the substrate 5′ hydroxyl group, (iv) ADP release and (v) dissociation of the 7 nt product strand (18). For the DRD26/2PT3.2 complex, the nucleic acid strands do not dissociate. Instead, the catalytic cycle is defined by four steps: (i) binding of ATPγS, (ii) thiophosphoryl transfer to a specific guanosine 2′ hydroxyl, (iii) ADP release and (iv) hydrolysis of the 2′ thiophosphate.

De-thiophosphorylation chemistry

Organic thiophosphates are normally much more stable than what we observe here for 2′-thiophosphorylated RNA. For example, 5′-thiophosphoryl groups on RNA and DNA remain attached for many hours at temperatures as high as 70°C in aqueous solutions that contain K^+ and Mg^{2+} (13). We have observed similar stability for 5′ thiophosphorylated RNAs incubated at 37°C in the selection buffer used to identify 2PT3.2 (data not shown). The 2′ thiophosphorylated RNA therefore behaves differently from RNA modified at the

5′ position. Similarly, substituted *O*-aryl phosphorothioates, such as 3,4-dinitro substituted or 4-nitro substituted benzyl phosphorothioates, were previously shown to be stable in aqueous solution (17,22,23), and Sekine *et al*. found that 2′ *O*-thiophosphate RNA derivatives were stable for >24 h in aqueous and non-aqueous solvents (24). However, none of these last experiments included any divalent metal ions, while the original selection of isolate 2PT3.2 included various alkaline earth and transition metal ions to provide the evolving library the opportunity to exploit the unique chemical reactivity of each ion (12).

The mechanism of 2′ de-thiophosphorylation is suggested by several observations of the parameters that regulate reactivity. First, the reaction does not require a specific secondary structure, proceeds normally in 8 M urea, and is inhibited by duplex formation and by self dimerization of the substrate strand, thus ruling out a ribozyme-catalyzed hydrolysis. Second, the reaction is highly dependent on the metal ions used in the assays, with significant stimulation by Mn^{2+} and low concentrations of soft transition metal ions. Third, in contrast to the de-thiophosphorylation reaction, hydrolysis of normal phosphate (from the product of a [^{32}P]ATP reaction) is essentially undetectable under similar reaction conditions (Figure 2A). Fourth, release of thiophosphate from 2′ modified RNA is much more rapid than release from 5′-modified RNA or DNA under similar conditions (13,18).

Each of these observations is consistent with a metal ion-catalyzed reaction in which the metal ion binds directly to the sulfur of the thiophosphate through inner sphere coordination. The metal ion may promote the reaction by reducing the negative charge density in the transition state, by stabilizing the leaving group, by increasing the electrophilicity of the phosphorous atom for attack by water, or by a combination of these effects. The metal ion may also interact with an adjacent backbone phosphate oxyanion, either through direct inner sphere coordination or by indirect outer sphere effects (Coulombic or water-mediated), either of which would serve to increase its occupancy at this site. This secondary coordination is not readily available at the 5′ end, which may contribute to the differential stability of 5′ versus 2′-thiophosphates. Coordination between the soft metal ion and soft ligand is eliminated when the transition metals are replaced by hard metals (such as magnesium), and when the thiophosphate is replaced by phosphate.

Potential conformational dynamics during the catalytic cycle

The 2PTmin3.2/DRD26 complex reproducibly attains ~60% thiophosphorylation upon extended incubations with ATPγS. Plateau values significantly <100% are commonly observed for other small ribozymes, and are usually interpreted to indicate either that the ribozyme is partially misfolded, or that both the forward and reverse reactions (e.g. cleavage and ligation for small nuclease ribozymes) contribute to establishing an internal equilibrium (25–27). A third possibility is that the complex arrives at a steady state between thiophosphorylation at the expense of ATPγS and de-thiophosphorylation to release thiophosphate. These models may contribute to some of the behavior of the DRD26/2PT3.2 complex. Although internal equilibration of the catalysis is ruled out—the reverse reaction (ATPγS synthesis) does not occur to an appreciable extent—the turnover rate of the annealed complex (~1–2 h^{-1}) is approximately an order of magnitude higher than the apparent forward rate of the reaction (0.21 h^{-1}, Figures 1C and 5), suggesting that the latter value probably reflects an approach to a steady state, rather than a true rate of thiophosphorylation.

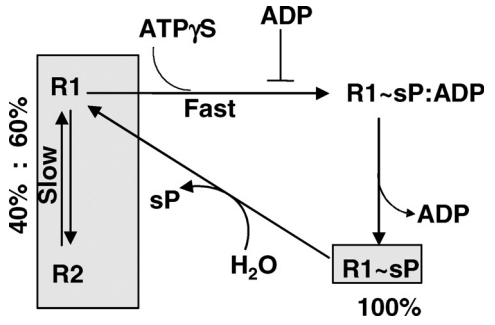

Figure 7. Reaction cycle for 'P-type ribo thioATPase.' Details of the model are given in the text.

However, these models fail to account for the lack of appreciable net de-thiophosphorylation in the presence of APTγS (Figure 5, triangles). An interesting possibility is that the persistence of a fully thiophosphorylated population may result from conformational dynamics of the ribozyme. Specifically, (thio)phosphorylation is proposed to lock the ribozyme into a catalytically active conformation, effectively preventing it from re-equilibrating into alternative, inactive states. A complex that assembles by incorporating an unmodified DRD26 strand is expected to equilibrate between active and inactive states, with ~60% in the active conformation (left side of Figure 7). In contrast, a complex that assembles by incorporating a pre-thiophosphorylated DRD26 strand is expected to fold essentially completely into the active complex (bottom right corner of Figure 7). If conformational re-equilibration is slow upon de-thiophosphorylation, the complex will be left for a short time in the catalytically competent conformation. During this time it can either re-thiophosphorylate rapidly without re-equilibration if ATPγS is present, (Figure 5, triangles), or it can slowly re-equilibrate between active and inactive conformations in the same 60:40 ratio as for the naïve complex if ATPγS is absent. Subsequent addition of ATPγS would then yield the same 60% product as that observed for naïve complex (Figure 5, circles).

The existence of a thio-ATP-powered catalytic cycle raises interesting possibilities for nucleic acid nanotechnologies. The active complex can clearly exist in at least two states during its catalytic cycle (with and without thiophosphate). If the angle and/or distance between the distal helical elements is altered by the presence of the (thio)phosphate—which seems likely given the introduction of bulk and charge—then the catalytic cycle could be used to transduce chemical energy into mechanical work. Additional kinase ribozymes that form 2′ thiophosphoryl intermediates (12,28,29) may be capable of similar cycles. A new challenge will therefore be to exploit this catalytic activity to capture the energy of ATPγS (or ATP) hydrolysis to drive otherwise unfavorable events, such as to power RNA-based molecular motors and nanodevices.

ACKNOWLEDGEMENTS

The authors thank members of the Burke lab for insightful comments on the manuscript. This work was supported by Exobiology Award NAG5-12360 from NASA and by an Interdisciplinary Science Award from the David and Lucille Packard Foundation. Funding to pay the Open Access publication charges for this article was provided by Exobiology Award NAG5-12360.

Conflict of interest statement. None declared.

REFERENCES

1. Burke,D.H. (2004) Ribozyme-catalyzed genetics. In Ribas de Pouplana,L. (ed.), *The Genetic Code and the Origin of Life*. Kluwer Academic/Plenum Publishers, London, p. 16.
2. Joyce,G.F. (2004) Directed evolution of nucleic acid enzymes. *Annu. Rev. Biochem.*, **73**, 791–836.
3. Jaschke,A. (2001) Artificial ribozymes and deoxyribozymes. *Curr. Opin. Struct. Biol.*, **11**, 321–326.
4. Tsukiji,S., Pattnaik,S.B. and Suga,H. (2003) An alcohol dehydrogenase ribozyme. *Nature Struct. Biol.*, **10**, 713–717.
5. Sengle,G., Eisenfuhr,A., Arora,P.S., Nowick,J.S. and Famulok,M. (2001) Novel RNA catalysts for the Michael reaction. *Chem. Biol.*, **8**, 459–473.
6. Liu,J. and Lu,Y. (2005) Stimuli-responsive disassembly of nanoparticle aggregates for light-up colorimetric sensing. *J. Am. Chem. Soc.*, **127**, 12677–12683.
7. Liu,J. and Lu,Y. (2005) Fast colorimetric sensing of adenosine and cocaine based on a general sensor design involving aptamers and nanoparticles. *Angew Chem. Int. Ed. Engl.*, **45**, 90–94.
8. Keiper,S., Bebenroth,D., Seelig,B., Westhof,E. and Jaschke,A. (2004) Architecture of a Diels-Alderase ribozyme with a preformed catalytic pocket. *Chem. Biol.*, **11**, 1217–1227.
9. Schlatterer,J.C., Stuhlmann,F. and Jaschke,A. (2003) Stereoselective synthesis using immobilized Diels-Alderase ribozymes. *Chembiochem*, **4**, 1089–1092.
10. Seelig,B. and Jaschke,A. (1999) A small catalytic RNA motif with Diels-Alderase activity. *Chem. Biol.*, **6**, 167–176.
11. Tarasow,T.M., Tarasow,S.L. and Eaton,B.E. (1997) RNA-catalysed carbon-carbon bond formation. *Nature*, **389**, 54–57.
12. Saran,D., Nickens,D. and DH,B. (2005) A *trans* acting ribozyme that phosphorylates exogenous RNA. *Biochemistry*, **44**, 15007–150016.
13. Rhee,S.S. and Burke,D.H. (2004) Tris(2-carboxyethyl)phosphine stabilization of RNA: comparison with dithiothreitol for use with nucleic acid and thiophosphoryl chemistry. *Anal. Biochem.*, **325**, 137–143.
14. Igloi,G.L. (1988) Interaction of transfer-RNAs and of phosphorothioate-substituted nucleic-acids with an organomercurial—probing the chemical environment of thiolated residues by affinity electrophoresis. *Biochemistry*, **27**, 3842–3849.
15. Miller,D.L. and Westheimer,F.H. (1966) The hydrolysis of gamma-phenylpropyl di- and triphosphates. *J. Am. Chem. Soc.*, **88**, 1507–1511.
16. Ramirez,F., Marecek,J.F. and Szamosi,J. (1980) Magnesium and calcium ion effects on hydrolysis rates of adenosine 5′-triphosphate. *J. Org. Chem.*, **45**, 4748–4752.
17. Herschlag,D. and Jencks,W.P. (1989) Evidence that meta-phosphate monoanion is not an intermediate in solvolysis reactions in aqueous-solution. *J. Am. Chem. Soc.*, **111**, 7579–7586.
18. Lorsch,J.R. and Szostak,J.W. (1995) Kinetic and thermodynamic characterization of the reaction catalyzed by a polynucleotide kinase ribozyme. *Biochemistry*, **34**, 15315–15327.
19. Geladopoulos,T.P., Sotiroudis,T.G. and Evangelopoulos,A.E. (1991) A malachite green colorimetric assay for protein phosphatase activity. *Anal. Biochem.*, **192**, 112–116.
20. Baykov,A.A., Evtushenko,O.A. and Avaeva,S.M. (1988) A malachite green procedure for orthophosphate determination and its use in alkaline phosphatase-based enzyme immunoassay. *Anal. Biochem.*, **171**, 266–270.
21. Van Veldhoven,P.P. and Mannaerts,G.P. (1987) Inorganic and organic phosphate measurements in the nanomolar range. *Anal. Biochem.*, **161**, 45–48.
22. Hollfelder,F. and Herschlag,D. (1995) The nature of the transition state for enzyme-catalyzed phosphoryl transfer. Hydrolysis of O-aryl phosphorothioates by alkaline phosphatase. *Biochemistry*, **34**, 12255–12264.
23. Herschlag,D. and Jencks,W.P. (1990) Catalysis of the hydrolysis of phosphorylated pyridines by $Mg(OH)^+$—a possible model for enzymatic phosphoryl transfer. *Biochemistry*, **29**, 5172–5179.
24. Sekine,M., Iimura,S. and Furusawa,K. (1993) Synthesis of a new class of 2′-phosphorylated oligoribonucleotides capable of conversion to oligoribonucleotides. *J. Org. Chem.*, **58**, 3204–3208.
25. Blount,K.F. and Uhlenbeck,O.C. (2002) Internal equilibrium of the hammerhead ribozyme is altered by the length of certain covalent cross-links. *Biochemistry*, **41**, 6834–6841.
26. Osborne,E.M., Schaak,J.E. and Derose,V.J. (2005) Characterization of a native hammerhead ribozyme derived from schistosomes. *RNA*, **11**, 187–196.
27. Stage-Zimmermann,T.K. and Uhlenbeck,O.C. (1998) Circular substrates of the hammerhead ribozyme shift the internal equilibrium further toward cleavage. *Biochemistry*, **37**, 9386–9393.
28. Curtis,E.A. and Bartel,D.P. (2005) New catalytic structures from an existing ribozyme. *Nature Struct. Mol. Biol.*, **12**, 994–1000.
29. Lorsch,J.R. and Szostak,J.W. (1994) *In vitro* evolution of new ribozymes with polynucleotide kinase activity. *Nature*, **371**, 31–36.